The Translation Initiation Factor Homolog, *eif4e1c*, Regulates Cardiomyocyte Metabolism and Proliferation During Heart Regeneration

A. Rao[1], B. Lyu[1], A. Lubertozzi[2], I. Jahan[1], Frank Tedeschi[3], Eckhard Jankowsky[3], B. Carstens[4], Ken Poss[5], K. Baskin[6] and J. Goldman[1*]

[1]The Ohio State University Medical Center, Department of Biological Chemistry and Pharmacology, Columbus OH

[2]The Ohio State University, Department of Molecular Genetics, Columbus OH

[3]Center for RNA Molecular Biology, Department of Biochemistry, School of Medicine, Case Western Reserve University, Cleveland, OH

[4]The Ohio State University, Department of Evolution, Ecology, and Organismal Biology, Columbus OH

[5]Duke Regeneration Center, Duke University School of Medicine, Durham NC

[6]The Ohio State University Medical Center, Department of Cell Biology and Physiology, Columbus OH

*corresponding author (aaron.goldman@osumc.edu)

1060 Carmack Rd
Rightmire Hall 105
Columbus, OH 43210
857-600-6488

Classification:
Biological Sciences
Developmental Biology, Evolution, Genetics

Abstract:

The eIF4E family of translation initiation factors bind 5' methylated caps and act as the limiting-step for mRNA translation. The canonical eIF4E1A is required for cell viability, yet other related eIF4E families exist and are utilized in specific contexts or tissues. Here, we describe a new family called Eif4e1c that is ancestral to the canonical eIF4E1A in vertebrates, and for which we find roles during heart development and regeneration in zebrafish. The Eif4e1c family is present in all aquatic vertebrates but has been lost in all terrestrial species. A core group of amino acids shared over 500 million years of evolution from ray-finned fish to sharks forms an evolutionarily conserved binding interface along the surface of the protein, suggesting Eif4e1c functions in a novel pathway. Deletion of *eif4e1c* in zebrafish caused growth deficits and impaired survival in juveniles. Mutants surviving to adulthood had fewer cardiomyocytes, while also showing reduced proliferative responses to cardiac injury. Ribosome profiling of mutant hearts demonstrated changes in translation efficiency of mRNA for genes known to regulate cardiomyocyte proliferation. Although *eif4e1c* is expressed in many tissues and is the predominant cap-binding initiation homolog in embryos, its disruption had most notable impact on the heart and at juvenile stages. Our findings reveal context-dependent requirements for translation initiation regulators during heart regeneration.

Significance Statement

Studies of gene expression during regeneration have focused on the abundance of mRNA transcripts. Here, we describe how translation is regulated to promote proliferation of cardiomyocytes during development and regeneration in zebrafish. The canonical cap binding protein, EIF4E1A, recognizes mRNA and stimulates ribosomes loading. Aquatic vertebrates have an ortholog called Eif4e1c that is lost in terrestrial vertebrates. Zebrafish mutants in *eif4e1c* have growth and survival deficits with smaller hearts, associated with reduced proliferation of cardiac muscle. They also display diminished cardiomyocyte cycling after injury. Dysregulation of translation in mutant hearts likely underlies these phenotypes. Identification of the novel ortholog *eif4e1c* as a factor in proliferation of cardiomyocytes is an unexpected finding with implications for how translation can stimulate heart repair.

Introduction:

Zebrafish regenerate heart muscle after catastrophic injury. Fervent research is underway to discover molecules that regulate fundamental events in regeneration and have potential relevance to regenerative medicine. Changes in the abundance of dozens to thousands of mRNAs have been reported using both targeted approaches like in-situ hybridization and unbiased approaches based on RNA-seq (1–3). However, reliance on mRNA as the sole measure of gene expression is an imperfect assumption at best, with only ~40% of mRNA levels correlating with the amount of protein (4). Similarly, the abundance of mRNA and proteins are poorly interconnected during heart regeneration, suggesting an important role for post-transcriptional regulation (5). An alternative snapshot of expression levels was revealed by profiling of mRNA bound to a transgenic ribosomal subunit (6), which uncovered a role for JAK/STAT signaling in heart regeneration. However, few total transcripts were identified, likely due to ribosome heterogeneities (7, 8), the dependence on transgenesis, and/or limited starting material. Regulation of translation is an important mechanism that impacts gene expression (9, 10) and is a central feature of physiologic heart growth (11). How such regulation might impact heart regeneration, however, remains largely unexplored until now.

Pathways that initiate translation are diverse, yet the classical means is through loading of the ribosome onto start codons via recognition of 5' methylated caps (12). The canonical eIF4E1A major cap binding protein is the rate-limiting factor to initiate loading, and its expression levels help determine the translation of specific mRNA cohorts (13, 14). In mouse, eIF4E1A, the canonical *Eif4e1a* gene, is essential for development and viability (15) limiting most mechanistic studies of its function to cell culture. However, studies of partial knockdowns and heterozygotes have shown *Eif4e1a* is generally found in excess and at reduced levels improves resiliency to cancer in heterozygous mice (14, 16) and indicated improved aging in adult worms (17). Actively growing heart muscle in neonatal mice has increased eIF4E1A levels (18), but how eIF4E1A is regulated in a context of innate heart regeneration is unknown. While the canonical eIF4E1A promotes translation, a second family of eIF4E1 homologs called eIF4E1B has been reported to have repressive functions (19, 20). In fish, a third close relative of canonical eIF4E1A, called *eif4e1c*, has been reported (21, 22), but its function and properties have not yet been described.

In a previous profiling study, we found that expression of the *eif4e1c* gene increases in zebrafish hearts during regeneration (2). We show that *eif4e1c* represents a new and highly conserved family of eIF4E1 that is retained in aquatic vertebrate and lost in terrestrial animals. The evolutionary changes that maintain heart regeneration in some organisms and not others is an area of intense study but with questions that still remain (23–26). Here, using CRISPR generated mutants, we demonstrate that fish-specific *eif4e1c* is required for normal proliferation of cardiomyocytes in zebrafish hearts during animal growth and injury-induced regeneration. Furthermore, our findings indicate that regulation of gene expression through translational mechanisms is a participating component of cardiogenesis.

Results and Discussion

Eif4e1c is a family of translation initiation factors conserved in all aquatic vertebrates

Zebrafish have two paralogs of the canonical eIF4E1A, *eif4ea* and *eif4eb*, that are likely a result of a whole genome duplication in teleost fish ~380 million years ago (27). Unlike the canonical eIF4E1A, zebrafish have only single copies of *eif4e1b* and *eif4e1c* (21) raising the possibility that they are duplicates of one another. Since the eIF4E1A and eIF4E1B families have distinct roles in translation (25, 26), the evolutionary history of *eif4e1c* may help inform its function. To understand the relationship of *eif4e1c* to the two other eIF4E1 families, we undertook a phylogenetic analysis of eukaryotic eIF4E1 orthologs. Using the IQ-TREE web server (28) we conducted a maximum likelihood analysis to estimate the phylogeny of 142 homologs from 53 species ranging from yeast to humans (*SI Appendix* Fig. S1*A*). Interestingly, Eif4E1c forms its own clade that is ancestral to the split of the Eif4e1a and Eif4e1b families (Fig. 1). A homolog of *eif4e1c* was found in all 37 aquatic vertebrates from this sampling including non-teleosts, suggesting that the Eif4e1c family predates the teleost specific duplication event. Whereas the Eif4e1a and Eif4e1b families are shared by aquatic and terrestrial vertebrate species, the Eif4e1c clade is absent from terrestrial animals. We conclude that the Eif4e1c family must have been lost in an early ancestor of terrestrial vertebrates but is retained in aquatic vertebrates.

To identify the sequence features that distinguish the Eif4e1c family we performed clustalW alignment between the four zebrafish homologs and their human orthologs (Fig. 2 *A*). All six homologs share the essential amino acids for binding 5' methylated caps (green) and assembly of the preinitiation complex with eIF4G (pink). In the 12 amino acids reported to distinguish eIF4E1A and eIF4E1B families (29), *eif4e1c* has substantially more similarity to eIF4E1A. For example, there are 7 residues identical or similar to canonical eIF4E1A (gray boxes) and 4 residues identical to the eIF4E1B variant (black boxes); however, of the 6 residues that confer optimal binding affinity for caps (red carrots), all 6 in *eif4e1c* share similarity with the canonical eIF4E1A. ClustalW alignment within the Eif4e1c family showed that the evolutionary conservation is striking (*SI Appendix* Fig. S1*B*). Shark and zebrafish Eif4e1c are 86% identical and 95% similar with only 8/186 substantial amino acid differences in the protein core over ~500 million years of evolution. There are 23 amino acids that are invariant in almost all Eif4e1c family members (Fig. 2 *A*, yellow boxes). Most of the 23 Eif4e1c residues are at locations in the protein where changes have been found and tolerated in other homologs from isolated species. Interestingly, 7 of the 23 amino acids remain identical in *all* eIF4E1A and eIF4E1B orthologs throughout evolution but are only different in the Eif4e1c family (red boxes). Thus, from amino acid sequence comparisons, we conclude that while Eif4e1c family shares features with the canonical eIF4E1A in critical cap binding residues, Eif4e1c is likely a unique homolog with both highly conserved and distinctive properties.

Crystal structures of eIF4E1A have been solved for several species showing that all homologs retain conserved features. To understand how the Eif4e1c distinctive residues may impact properties of the protein, we modeled zebrafish Eif4e1c over a crystal structure of human EIF4E1A bound to a capped GTP residue and a peptide from EIF4G (30) using RoseTTA fold (Fig. 2 *B*) (31). The canonical folds of the Eif4e1c protein are identical to what is found in the core of all eIF4E1 family members, with similar positioning of the two highly conserved tryptophans required for cap binding and preinitiation complex assembly (yellow). This mirrors what is seen in the Alphafold prediction of the two molecules (32). The 23 amino acids

characteristic of the Eif4e1c family are positioned mainly along the protein surface in solvent exposed regions. A distinctive Eif4e1c specific patch is found opposite the EIF4G binding site and adjacent to the cap-binding region. Therefore, the highly conserved amino acids shared by the Eif4e1c family create a novel binding interface on the protein, suggesting that *eif4e1c* interacts with unique partners.

The *eif4e1c* gene is widely expressed in tissues and throughout development

Canonical eIF4E1A and eIF4E1B are known to have distinct expression patterns. For example, *eif4e1b* is only expressed in the gonads and skeletal muscle in adults and during the first 12 hours-post-fertilization (hpf) (19). To determine if *eif4e1c* is expressed in all tissues like eIF4E1A or is restricted to discrete organs or developmental stages like *eif4e1b*, we evaluated expression of *eif4e1c* in heart, fin, skeletal muscle, spleen, brain, and liver using RT-qPCR. Each of *eif4ea, eif4eb,* and *eif4e1c* genes were expressed in every organ examined but to varying degrees (Fig. 2 *C*). Canonical *eif4ea* was found highest in the spleen; 23 times more than the lowest expressing tissue, skeletal muscle. Canonical *eif4eb* was found highest in the brain; 11 times more than the lowest expressing organ, the liver. The *eif4e1c* homolog is expressed in every tissue examined, highest in the heart and brain, 3.4 and 5.5 times higher than the fin where expression is the lowest. Thus, in adult tissues *eif4e1c* is broadly expressed similar to the canonical orthologs *eif4ea* and *eif4eb*.

Using the EMBL expression atlas, we assessed expression levels of all eIF4E1 orthologs during a time course across early zebrafish development (33). Zebrafish *eif4e1c* is the most highly expressed eIF4E1 at every time point during the first five days of development, during which most organ systems are formed (Fig. 2 *D*). Expression levels of *eif4e1c* are roughly equal to the sum of both *eif4ea* and *eif4eb* except during the first 12hpf where *eif4e1c* is 3-4X more abundant. In adult hearts, RNAseq analysis showed that *eif4e1c* is expressed at levels similar to canonical *eif4ea* and *eif4eb* (2). By normalizing qPCR signal from other tissues to the heart we extrapolate that *eif4e1c* is expressed at similar levels to the canonical paralogs in most tissues except for the liver, which has ~5X less *eif4eb* and the spleen which has ~6X more *eif4ea* (Fig. 2 *C*). During rapid growth stages such as during embryogenesis, *eif4e1c* is the dominantly expressed cap-binding homolog but is expressed mostly at similar levels as canonical factors in the adult.

Taken together, Eif4e1c is an aquatic vertebrate specific homolog of canonical eIF4E1A, that retains critical amino acids and broad expression patterns unlike other previously reported homologs (20, 29, 34, 35). In addition, *eif4e1c* likely has specific functions within a pathway distinct from the canonical homologs as indicated by its unique structural features (Fig 2 *B*).

Deletion of the *eif4e1c* locus causes poor growth and survival to adulthood

Eif4e1a in mice is required for viability with no detectable homozygous mutant mice from heterozygous crosses (15). To examine whether *eif4e1c* is essential in the zebrafish system, we generated a stable CRISPR mutant fish line with an *eif4e1c* deletion, hereafter referred to as Δ*eif4e1c*. Using guide RNA's targeting flanking loci, we created a 12,131bp deletion in the *eif4e1c* gene extending from intron 1 to exon 7 and deleting the entire coding region (Fig. 3 *A*). Crosses between Δ*eif4e1c* heterozygotes yielded larvae at 3 days-post-fertilization (dpf) in normal Mendelian ratios (Fig. 3 *B*). One possibility is that embryonic fish develop through early stages due to maternal deposition of wildtype *eif4e1c* mRNA or protein (36). Thus, we crossed

homozygous Δ*eif4e1c* mutant females with heterozygous Δ*eif4e1c* males and still found Mendelian ratios in the progeny, eliminating a contribution of maternal deposition (58+/- : 49-/-). Mutants were found at normal Mendelian ratios through early juvenile stages up to 4 weeks-post-fertilization (wpf) (chi^2 = 0.629, p value = 0.73). Beginning in late juvenile stages, 8wpf, heterozygotes and homozygous mutants are underrepresented among the progeny (599+/+ : 951-/+ : 318-/-, chi^2 = 29.3, p value = 4.31×10^{-7}). Although homozygous Δ*eif4e1c* fish were recovered in adults at 3 months-post-fertilization (mpf), survivorship was diminished in mutants and heterozygotes (Fig. 3 *B*, chi^2 = 84.9, p value = 3.22×10^{-19}). Therefore, deletion of *eif4e1c* is not embryonically lethal but begins to influence viability between 4-8wpf with only ~80% of heterozygotes and ~50% of homozygote mutants surviving past 8wpf.

Throughout all stages of development Δ*eif4e1c* mutants appear visibly normal morphologically but Δ*eif4e1c* mutant adults have notable size differences suggesting impaired growth. At 3mpf, Δ*eif4e1c* mutant fish were 12% shorter (mean length wt = 1.816cm, mutant = 1.622cm, p-value= 0.0156, n=24 vs 25; Fig. 3 *C*) with 30% lower mass (mean= 146.5mg, 103.1mg, p-value= 0.0014, n=24, 25; Fig. 3 *D*). Similar results were found when males and females were considered separately. The weight difference persists in older fish (6mpf) (Fig. 3 *D*; mean= 344.6mg, 261.7mg, p-value= 0.0002, n= 20, 20) but the length difference resolves (Fig. 3 *C*; mean= 2.480cm, 2.370cm, p-value= 0.0708, n= 20, 20). Heterozygous Δ*eif4e1c* carriers did not demonstrate a significant length or weight difference as adults (*SI Appendix* Fig. S2*A*). We conclude that Δ*eif4e1c* homozygous fish have reduced growth that persists into adulthood.

To determine if apparent growth defects reflect fewer overall cell numbers, we quantified CM numbers using an antibody for a nuclear marker of cardiac muscle (Mef2c). CM content was compared between adult hearts (3mpf) of Δ*eif4e1c* mutant fish and their wildtype siblings. Mutant heart ventricles had 25% fewer CMs compared to their WT siblings (mean: WT= 3070, mutant = 2432, p-value= 0.0055, n=7, 7; Fig. 4 *E*). At 6mpf, mutant heart ventricles were also smaller demonstrating that fewer CMs during development are not rescued by regeneration mechanisms in the adult (*SI Appendix* Fig. S2*B*). Therefore, deficits in overall growth in adult *eif4e1c* mutants likely reflect defects in proliferation or cell survival during development.

In contrast to reported *Eif4e1a* mutants in mice, zebrafish *eif4e1c* deletion knockouts can survive (15, 37). Similarities in sequence and expression patterns between *eif4e1c* and its canonical homologs *eif4ea* and *eif4eb* raises the possibility that Δ*eif4e1c* mutants survive because the canonical homologs can functionally substitute. However, if canonical *eif4e1a* homologs allow Δ*eif4e1c* mutants to develop, it is not clear why they do not also compensate in juveniles and adults. The conclusion that reduced total expression of *eif4e1a* paralogs would underlie growth deficits in Δ*eif4e1c* mutant adults is also not supported by studies in other organisms. A wide array of lower expression levels from canonical eIF4E1A knockdown experiments demonstrated that 50-70% less protein is tolerated without obvious phenotypes in growth (14, 16). These observations led us to hypothesize that the *eif4e1c* ortholog is specialized and functions to foster growth in juveniles and adults, a phenomenon commonly observed in aquatic species. From the reduced body size of Δ*eif4e1c* mutants we speculate that loss of the Eif4e1c family in early terrestrial vertebrates may have limited growth in adults as an adaption to survival on land.

Ribosome profiling of Δ*eif4e1c* mutant hearts uncovers translational changes

The eIF4e1 family core amino acids responsible for initiating loading of ribosomes for translation are conserved in zebrafish Eif4e1c. Therefore, we hypothesized that the survival and growth deficits that occur upon deleting *eif4e1c* result from alterations in translation. To look for changes in the translatome we performed ribosome profiling which entails sequencing mRNA fragments protected by virtue of being bound to the ribosome (Fig. 4 *A*). Therefore, the level of ribosome protected fragments (RPF) can illuminate the translational status of a transcript. Normalization of ribosome profiling to the total amount of transcript (RNAseq) provides a quantitative measure of translational efficiency that can be compared between conditions. Since, Δ*eif4e1c* mutants have small hearts as adults, we performed ribosome profiling to compare the translatome of adult 3mpf Δ*eif4e1c* mutant hearts to that of their wildtype siblings. Overall, there were 129 genes with transcripts that are less efficiently translated and 197 genes with transcripts that are more efficiently translated in the Δ*eif4e1c* mutant (Fig. 4 *B*). Thus, deletion of the *eif4e1c* gene resulted in translational changes in almost one fifth (19.6%) of the total expressed genes detected by ribosome profiling in adult hearts.

Several of the translationally misregulated transcripts in Δ*eif4e1c* mutant hearts could explain some of the observed phenotypes. For example, *stat3* activity is required for CM proliferation during heart regeneration (6) and translation efficiency of *stat3* mRNA is 2.9-fold lower in Δ*eif4e1c* mutant hearts (Fig. 4 *C*). Retinoic acid signaling is also required for CM proliferation during development (38) and regeneration (39) and translational efficiency for a transcription factor downstream of retinoic acid signaling called *zic2b* is 3.1-fold lower in mutant hearts (Fig. 4 *B*). Gene ontology (GO) analysis using the DAVID platform (40, 41) revealed genes encoding cell cycle proteins were significantly enriched among transcripts with lower translation efficiency (*SI Appendix* Fig. S3*A*). Included, are *mapre1a* that associates with the AuroraB kinase to assemble microtubules during cytokinesis (42) and *cdc123* which encodes a translation factor required for eIF2 assembly, a complex needed for protein synthesis initiation and cell cycle progression (43, 44). Thus, deletion of *eif4e1c* led to decreased translation of mRNA encoding signaling pathways that promote CM proliferation and cell division in uninjured hearts.

Other *eif4e1c*-dependent changes in translation may occur at time points closer to 4wpf just when mutants first begin to die. Ribosome profiling at these stages is not possible since zebrafish hearts are quite small, difficult to isolate and do not yield the amount of starting material required. By 12wpf translational buffering (45, 46) from other cap-binding proteins or other genetic compensation may mask some of the *eif4e1c* affected transcripts. Compensatory changes may also support the 50% mutant survival beyond 4wpf. For example, we detected *increased* translational efficiency of transcripts encoding pro-growth factors in Δ*eif4e1c* mutant hearts. A receptor for the potent CM mitogen Nrg1 (47–49) called *errb4a*, is translated 1.57-fold more efficiently by ribosome profiling. Also, translated more efficiently are Fgf family members (*fgf8b* - 2.96-fold, *fgf12a* - 31.59-fold, *fgf19* - 2.38-fold) that have been reported to be pro-survival and pro-proliferative to CM (50–52). Reduced mitochondrial activity has been reported to be pro-proliferative in the heart (1, 53–55). Translated more efficiently are transcripts encoding ucp1 (3.75-fold), a mitochondrial uncoupling factor reduces mitochondrial activity to mitigate production of reactive oxygen species (56). In sum, even though translation

efficiency of of pro-growth pathways and molecules in Δ*eif4e1c* mutant hearts is enhanced, mutant hearts are still deficient in growth (Fig. 3 *E*). This strongly suggests that increased translation of pro-growth pathways is compensatory and activated to mitigate *eif4e1c* loss in hearts. We conclude that *eif4e1c* is critical for heart growth but that other less efficient pro-growth pathways can partially compensate for *eif4e1c* loss likely through the remaining *eif4e1* canonical orthologs.

To examine the biological significance of increased *ucp1* translation we measured oxygen consumption rates (OCR) of mitochondria isolated from hearts using the Agilent Seahorse bioanalyzer Agilent (*SI Appendix* Fig. S3*B*). Mitochondria from Δ*eif4e1c* mutant hearts had lower OCR compared to the mitochondria from wildtype sibling hearts (Fig. 4 *D*). The basal and maximal respiration rates of mutant hearts were significantly lower (25.59% and 24.06%, respectively), which suggests impaired mitochondrial output (Fig. 4 *E*). To examine whether reduced mitochondrial activity is also observed by the Seahorse during heart growth, we compared respiration of mitochondria from uninjured hearts to mitochondria from regenerating hearts using the Seahorse analyzer. In agreement with a previous report (1), mitochondrial activity plummets in zebrafish hearts undergoing regeneration with basal respiration decreasing 75.5% and maximal respiration decreasing 62.0% (*SI Appendix* Fig. S3*C-E*). Since reduced mitochondrial activity correlates with growing heart muscle, a similar but less profound reduction in mitochondrial activity in Δ*eif4e1c* mutants may function as a mechanism to foster compensatory growth.

Ribosome profiling demonstrated that translational changes occur in Δ*eif4e1c* mutant hearts but it is unlikely that every transcript is a direct Eif4e1c target. Second order effects are likely considering that three of the top five dynamic transcripts encode transcription factors. Moreover, if compensation drives survival in Δ*eif4e1c* mutants, then it is likely that some Eif4e1c-bound transcripts are not affected in our ribosome profiling experiment. Nevertheless, many translational changes *are* detected in hearts of Δ*eif4e1c* mutant hearts, including some that may explain their smaller heart size.

Deletion of *eif4e1c* impairs metabolic remodeling and regeneration in the heart

We hypothesized that increased expression of *eif4e1c* mRNA in regenerating hearts may stimulate heart growth during regeneration (2). After surgical removal of the apex of the heart, Δ*eif4e1c* mutants had diminished CM proliferation during the peak of heart regeneration compared to wildtype siblings (Fig. 5 *A*). The fraction of *Mef2c* positive CMs that were also positive with the proliferation marker EdU was reduced by 35% seven days post amputation (dpa) of the ventricular apex (mean=10.68%, 6.897%, p-value= 0.0360, n = 11, 14). However, homozygous Δ*eif4e1c* mutants did complete regeneration despite early defects in CM proliferation and look the same as their wildtype siblings by 28dpa (*SI Appendix* Fig. S4*A*). Thus, we conclude that Δ*eif4e1c* mutants have impaired CM proliferation that may be resolved by compensatory mechanisms at later stages of regeneration.

As previously discussed, regulation of mitochondrial respiration is a feature of heart regeneration that promotes growth. One of the key enzymes central to connecting the TCA cycle to the electron transport chain is succinate dehydrogenase (Sdh); Sdh activity is reported to be sharply downregulated during heart regeneration (1, 57). Using the ZCAT, a transgenic system

to ablate CMs, we too found Sdh activity to be reduced during regeneration (Fig. 5 *C*). While Δ*eif4e1c* mutant hearts also have lower Sdh activity, Sdh activity was higher in Δ*eif4e1c* mutant hearts compared to their wildtype siblings (Fig. 5 *D*). For uninjured hearts, Sdh activity was unchanged. This suggests that an inability to fully reduce Sdh activity may in part underlie the impairment of heart regeneration in Δ*eif4e1c* mutants. It is unclear if the *sdh* transcript is a direct target of *eif4e1c* or if changes in its activity are regulated indirectly.

After development, Δ*eif4e1c* mutants had deficiencies in overall length (Fig. 3 *C*). To determine whether this impaired growth extends to regeneration, we analyzed the ability of Δ*eif4e1c* mutants to regenerate their fins. Fin regeneration was determined by measuring growth of caudal fins in Δ*eif4e1c* mutants and their wildtype siblings 4 days post amputation (Fig. 5 *E*). There is no significant difference in fin regrowth indicating that Δ*eif4e1c* mutants can normally regenerate their fins (Fig. 5 *F*, mean=849.6μm, 857.2μm, p-value=0.8605, n=30, 25). Using RT-qPCR, we found that like in the heart, *eif4e1c* abundance does increase 2.3X in the blastema of caudal fins (*SI Appendix* Fig. S4*C*); yet the overall expression is still lower than in the heart. Interestingly, unlike the heart, canonical *eif4eb* is upregulated during fin regeneration suggesting other translational pathways beyond those regulated by *eif4e1c* are likely more critical in the fin (*SI Appendix* Fig. S4*C* and *D*). Thus, deletion of *eif4e1c* causes general growth defects in adults but its effects on regeneration do not extend to all tissues.

This study establishes a new pathway for translational regulation mediated by a homolog of an mRNA cap-binding protein called *eif4e1c*. This pathway is highly conserved in aquatic species but lost in terrestrial vertebrates. Importantly, we show that in zebrafish, *eif4e1c,* is required normal cardiogenesis during development and regeneration. While *eif4e1c* is broadly expressed both during development and in adults, overt mutant phenotypes are restricted to particular tissues and first observed in juveniles. For example, heart regeneration, but not fin regeneration, is impaired. Likely, specific features of the Eif4e1c protein allow for targeting distinct cohorts of transcripts that underlie the different tissue sensitivities found during regeneration. The data presented here suggests that regulation of metabolism may be an aspect of *eif4e1c* function that predisposes heart muscle to a reliance of *eif4e1c*. Alternative pro-CM growth pathways not dependent on *eif4e1c* exist, as Δ*eif4e1c* mutants do complete regeneration albeit with a reduced index of CM proliferation. In the future, determining a contribution to regeneration for each of the canonical mRNA cap-binding proteins will help construct a translation regulatory network for heart regeneration with possible therapeutic implications.

Materials and Methods

Phylogeny of the Eif4e1c family – Expanding on previous studies, we analyzed 20 species of teleosts covering most if not all subclades (58) including the most ancestral species Asian arowana (*S. formosus*) (59) and the spotted gar (*L. oculatus*) (60). Beyond teleost we also included multiple species of sharks, rays, eels, and the fish that are the closest relatives to terrestrial tetrapods like mudskippers (*P. magnuspinnatus*) (61) and lungfish (*P. senagalus*, *P. annectens*) (62). Phylogenetic analysis was conducted using maximum likelihood as an optimality criterion as implemented in IQ-TREE2 (63). The JTT+G (4 state) model of amino acid substitution was selected using corrected Akaike Information Criterion (AIC) scores and used to estimate the phylogeny. Branch support was estimated using 1000 replicates of the ultrafast bootstrap with a minimum correlation coefficient of 0.99. IQ-TREE search parameters include a perturbation strength of 0.5 for the randomized nearest neighbor interchange with >100 unsuccessful iterations required to end the heuristic search of tree space. All analyses were conducted using the IQ-TREE web server (28).

Gene expression analysis by RT-qPCR – Dissected tissues were placed in Hank's Buffered Salt Solution and washed three times in PBS before being snap frozen. For regenerating fins, only the blastema was removed. Organs from 10 fish were pooled (5 male, 5 female). Primer pair efficiency was assessed and validated to be 95%-105%. RNA was isolated using an adapted version of a published protocol and then DNased (64). Reverse transcription (RT) was performed with 1ug toRNA using SuperscriptIII (Thermo) and qPCR was performed with 3 technical replicates for each condition. Controls without RNA template in the RT were run for each primer pair to identify possible DNA contamination and none was found. Fold gene expression was determined using the ΔΔCt method and normalized to *mob4* (65).

Construction of *eif4e1c* deletion fish line – Guide RNAs (sgRNA) were designed against intron 1 (GGACATGTTTAAGCAGTGAG) and exon 7 (CAGAGGCACCTGCAGACTGA). DNA templates of the respective sgRNA fused to a tracRNA were produced by PCR. T7 transcribed sgRNA were then injected with Cas9 protein into newly fertilized embryos from EK parents. Adults injected at fertilization were mated and embryos of possible stables lines were screened by PCR oligos (Fwd: CGGTAAGAGGGATCGGGCTTGGT, Rev: GTCTACAAGCAAGATGCCACAATTCCAGCA) flanking the deleted region (chr13:18,311,769:18,323,899). The selected line, called *eif4e1c*^{pd370} was a perfect deletion without addition of extra nucleotides between the fused cut sites. Heterozygote adults were mated as described.

Length and weight measurements – 3-6mpf zebrafish were anesthetized in phenoxyethanol and their length was measured using a ruler starting from the eye to the center of caudal tail fin before the lobes diverge. After removing excess water with a Kimwipe, the anaesthetized zebrafish were weighed on an analytical scale. Fish were with different genotypes were raised and housed together and measured shortly after genotyping.

Immuno-histochemistry - Primary antibodies used in this study were anti-Mef2 (1:100, Abcam ab197070) and anti-MF20 (1:100, DSHB MF20). Secondary antibodies were, anti-mouse Alexa546 (1:200) for MF20, and anti-rabbit-Alexa488 (1:200) for Mef2. Three sections representing the hearts with largest lumen were selected from each heart and imaged using a 20X objective on a Zeiss confocal. For obtaining cardiomyocyte counts, the number of Mef2c+ nuclei were counted using MIPAR image analysis software (Sosa).

Ribosome profiling – For each replicate sample, RNA from thirty zebrafish hearts was extracted for Ribo-seq library generation and parallel RNA-seq. The hearts were lysed on ice with 100ul of lysis buffer with 53 mg/ml cycloheximide using mechanical homogenization with a pestle for thirty seconds. Cells were lysed further by trituration of the sample using a 27.5-gauge needle syringe 20x on ice. Cell extracts (average OD 7) were treated with MNase (NEB), $CaCl_2$ (5mM final concentration), and Turbo DNAse I (Invitrogen) at 25°C for 30 minutes. MNase digestion was stopped with SUPERase-inhibitor incubation on ice. 80S ribosomes were isolated using SH400 spin columns (Cytiva). Columns were prepared according to the manufacturer's instructions. 100 µls of MNase treated sample was loaded per column and centrifuged for 2 min at 600 RCF. The flow through was isolated and incubated for 5 min. with 3x volume of Trizol LS (Ambion). 200 µl of chloroform was added and incubated for 2 min. Samples were centrifuged for 15 min. at 12,000 rpm (4°C). The aqueous phase was extracted and precipitated overnight at -20°C using glycoblue (ThermoFisher) and isopropanol followed by centrifugation for 30 minutes at 4C at 10,000 RPM. Pellets were washed with 75% Ethanol and resuspended into RNase free water (66).

Samples were subjected to 15% denaturing polyacrylamide-mediated gel (UreaGel 29:1 gel system, National Diagnostics) and visualized by SYBR gold (ThermoFisher) after electrophoresis. Ribosome-protected RNA fragments 26-mers to 34-mers were excised and RNA was eluted overnight by rotating the gel slices in RNA extraction buffer (300 mM NaOAc (pH 5.2), 1mM EDTA, 0.25% (w/v) SDS at room temperature. To deplete rRNA fragments, the isolated RNA was precipitated on dry ice for 30 minutes using glycoblue (ThermoFisher) and isopropanol and treated with the RiboMinus Ribosomal RNA depletion kit (Ambion), according to the manufacturer's instructions.

The RNA samples were then de-phosphorylated by adding 1ul of T4 PNK, 1ul SUPERase-In, 7ul of 10X PNK reaction buffer for a 70ul volume reaction. The reaction is incubated then for 1 hour at 37C before adding 1ul of 100mM ATP for 30 minutes at 37C. The reaction is then heat inactivated at 70C for 10 minutes and precipitated as before. Adapter ligation, reverse transcription and subsequent cDNA amplification were performed using the NEXT-Flex smRNA-Seq Kit v3 (Perkin Elmer). Samples were subjected to 8% native PAGE (0.5X TBE) gel electrophoresis. cDNA products of the final PCR were visualized by SYBR gold (ThermoFisher), excised from the gels, and extracted overnight with DNA extraction buffer (300 mM NaCl, 10mM Tris (pH 8.0), 1 mM EDTA) and precipitated as described previously.

To prepare RNA-seq libraries, total RNA was isolated from each sample using Trizol LS as described above and subjected to Turbo DNase I digestion (1ul Turbo Dnase 1, 1x DNase reaction buffer, 20 minutes at 37C). RNA-seq libraries were constructed from 500ng of purified RNA using Illumina's TruSeq Stranded Total RNA kit, according to the manufacturer's instructions, by the Case Western Reserve University (CWRU) Genomics Core.

Libraries were assessed for quality by Agilent Bioanlyzer followed subsequently by single-end 75 cycle sequencing. The RNA-seq and Ribo-seq sequencing was performed at the CWRU Genomics Core on the Illumina NEXTseq 550 v2.5 (High Output) platform.

Bioinformatics

Ribosome profiling – Fastq files were processed using FastQC (v0.11.8; RRID:SCR_014583) for quality control (QC) analysis. Pre-processing of sequencing reads was based on the QC report using the FASTQ Quality Filter module in the FASTX-Toolkit (RRID:SCR_019035). This was used to filter the bases with 99% accuracy based on Q Score. Reads were removed that showed less than 70% of nucleotides with an accuracy of at least 99%. The sequences were collapsed according to their by Unique Molecular Identifiers (UMIs). Cutadapt

(RRID:SCR_011841) was used to trim 21-nt adaptor before the first nt and the last 4 nt from the reads to remove the UMI.

The processed reads were aligned to GRCz11/danRer11 (assembly of the zebrafish genome; Genome Reference Consortium) using STAR v2.5.3a (RRID:SCR_004463). Sequencing replicates were highly similar to one another for both ribosome protected fragments and input mRNA (*SI Appendix* Fig. S5*A*). Generated bam files were processed with RiboProfiling package v1.2.2 (67). Coverage counts on the coding regions (CDS) were obtained for each sample based on RiboProfiling function modules, *TxDb.Drerio.UCSC.danRer11.refGene (*v3.4.6; Annotation package for TxDb object(s); Team BC, 2019) and GenomicFeatures package v1.46.1 (68). Differential expression analysis was performed using the DESeq2 pipeline (version 1.26.0), based on the expressed raw reads (69). Statistic thresholds for the features in the comparison results (p-values and log2 fold changes), were used for the gene extraction, as described.

Genes with transcripts with increasing translation efficiency in mutant hearts were calculated as (1) significantly increasing by RPF and not mRNA, (2) not significantly increasing by RPF but significantly decreasing by mRNA or (3) significantly changing in both datasets with an RPF/mRNA ratio > 1. Genes with transcripts translated less efficiently were identified as (1) decreasing significantly by RPF and not changing by mRNA, (2) not significantly changing in RPF but significantly increasing in mRNA, or (3) significantly changing in both datasets with an RPF/mRNA ratio < 1. Gene ontology categories were identified using DAVID (40, 41).

Zebrafish cardiac regeneration experiments - Zebrafish were anesthetized using Tricaine and placed ventral side up on a sponge to carry out resection of the ventricular apex. Iridectomy scissors were used to make an incision through the skin and pericardial sac. Gentle abdominal pressure exposed the heart and ~20% of the apex was removed with scissors, penetrating the chamber lumen (70). Hearts were harvested 7, 14 or 30 days after injury depending on the experiment. To genetically ablate cardiomyocytes, *cmlc2:CreER*^{pd10}*; bactin2:loxp-mCherry-STOP-loxp-DTA*^{pd36} (Z-CAT) fish were incubated in 0.5 μM tamoxifen for 17 hours (71).

To quantify CM proliferation – Injured fish were injected into the abdominal cavity once every 24hrs for 3days (4-6dpa) with 10ul of a 10mM solution of EdU diluted in PBS. Hearts were removed on day 7, embedded and cryo-sectioned. Slides were stained with Alexa594-azide using CLICK chemistry and then immunostained for Mef2c. Briefly, sections were blocked with 1% BSA (Fraction V) and 5% goat serum and washed in PBS with .2% triton-100. Three sections representing the largest wound area were selected from each heart and imaged using a 20X objective. The number of Mef2+ and Mef2+EdU+ cells were counted using the MIPAR image analysis software and the CM proliferation index was calculated as the number of Mef2+EdU+ cells / total Mef2+ cells (Sosa). The CM proliferation index was averaged across 2-4 appropriate sections from each heart.

To visualize regrowth - Hearts were removed 28dpa, embedded and cryo-sectioned. Slides were incubated at 60 °C for 3 h in Bouin-fixative previously heated at 60 °C for 30 min. Slides were then rinsed in distilled water (dH_2O) for 30 min, and then incubated with 1% (w/v) phosphomolybdic acid solution for 5 min. Following a 5 min wash-step in dH_2O, sections were stained with the AFOG-solution for 5 min, washed, dehydrated and then mounted in Cytoseal. Three sections representing the largest wound area were selected from each heart and imaged using a 20X objective.

Fin regeneration analysis – Fish were anesthetized in phenoxyethanol, and the caudal fins were amputated just below bifurcations of rays using a razor blade and removing ~1/2 of the fin from body to tip. Animals were allowed to regenerate for 4 days after which fins were imaged using a 10X objective. Fin regrowth was measured from the amputation till the tip of each ray using the Zeiss microscope software. The 2nd through 4th rays were averaged from both the dorsal and ventral sides.

Seahorse analysis of mitochondrial respiration – Mitochondria from fish hearts were isolated as previously described in mice (72). Oxygen consumption rates were optimized for 1.5μg of mitochondria which were resuspended in respiratory buffer (70mM sucrose, 220mM mannitol, 10mM K2HPO4, 5mM MgCl2, 2mM HEPES, 1mM EGTA, pH 7.4. Electron coupling (EC) assays were performed using the Seahorse Bioanalyzer (Agilent). The EC assay measures basal respiration in coupled mitochondria with substrates present (succinate/rotenone), but no ADP, which drives respiration through electron transport chain (ETC) complexes II-IV. Active respiration is initiated by addition of ADP to mitochondria, increasing OCR. Oligomycin, an ATP synthase/Complex V inhibitor, decreases OCR. FCCP, an ETC chemical uncoupler, allows for maximal uncoupled respiration. Antimycin A, which inhibits complex III, shut down electron flow, ATP production, and OCR. Proton leak through the ETC can be determined with oligomycin treatment, and spare respiratory capacity is the difference in maximal respiration (FCCP treatment) and protein leak (Oligomycin treatment). After Seahorse measurements, the abundance of mitochondria was verified using qPCR and used to normalize the readings.

SDH staining – Hearts were embedded fresh and sectioned and stained the same day. The succinate dehydrogenase (Sdh) enzymatic activity was measured by incubating sections with 37.5 mM sodium phosphate buffer pH 7.60, 70 mM sodium succinate, 5 mM sodium azide and 0.4 mM tetranitro blue tetrazolium (TNBT) for 20 min at 28°C (1). The reaction was quenched in 10 mM HCl and slides were mounted in glycerin-gelatin mounting media. Images were processed with ImageJ calculating percent mean intensity of signal averaged by the total area of the heart (pixels).

Acknowledgements

We would like to thank the Busch-Nentwich lab for providing RNA-seq data from zebrafish embryos (http://www.ebi.ac.uk/gxa/experiments/E-ERAD-475). Confocal imaging was performed in the Neuroscience Imaging Core at OSU, made possible by NIH Shared Instrumentation Grant (S10 OD026842). Thanks to Charles Bell and Tianmin Fu who helped guide the structural modeling. We acknowledge funding from NIH grant R35HL150713 for K.D.P. and from an American Heart Association grant 17SDG33660922 and the Department of Biological Chemistry and Pharmacology for J.A.G.

REFERENCES

1. H. Honkoop, *et al.*, Single-cell analysis uncovers that metabolic reprogramming by ErbB2 signaling is essential for cardiomyocyte proliferation in the regenerating heart. *Elife* 8, e50163 (2018).

2. J. A. Goldman, *et al.*, Resolving Heart Regeneration by Replacement Histone Profiling. *Dev Cell* 40, 392 404.e5 (2017).

3. C.-C. Wu, *et al.*, Spatially Resolved Genome-wide Transcriptional Profiling Identifies BMP Signaling as Essential Regulator of Zebrafish Cardiomyocyte Regeneration. *Dev Cell* 36, 36–49 (2016).

4. C. Buccitelli, M. Selbach, mRNAs, proteins and the emerging principles of gene expression control. *Nat Rev Genet* 21, 630–644 (2020).

5. D. Ma, *et al.*, Dynamics of Zebrafish Heart Regeneration Using an HPLC–ESI–MS/MS Approach. *J Proteome Res* 17, 1300 1308 (2018).

6. Y. Fang, *et al.*, Translational profiling of cardiomyocytes identifies an early Jak1/Stat3 injury response required for zebrafish heart regeneration. *Proc National Acad Sci* 110, 13416 13421 (2013).

7. E. Emmott, M. Jovanovic, N. Slavov, Ribosome Stoichiometry: From Form to Function. *Trends Biochem Sci* 44, 95–109 (2018).

8. N. R. Genuth, M. Barna, Heterogeneity and specialized functions of translation machinery: from genes to organisms. *Nat Rev Genet* 19, 431 452 (2018).

9. Z.-Y. Wang, *et al.*, Transcriptome and translatome co-evolution in mammals. *Nature* 588, 642–647 (2020).

10. J. Kong, P. Lasko, Translational control in cellular and developmental processes. *Nat Rev Genet* 13, 383–394 (2012).

11. S. Chorghade, *et al.*, Poly(A) tail length regulates PABPC1 expression to tune translation in the heart. *Elife* 6, 568 (2017).

12. K. L. B. Borden, L. Volpon, The diversity, plasticity, and adaptability of cap-dependent translation initiation and the associated machinery. *Rna Biol* 17, 1–13 (2020).

13. M. R. Davis, M. Delaleau, K. L. B. Borden, Nuclear eIF4E Stimulates 3'-End Cleavage of Target RNAs. *Cell Reports* 27, 1397 1408.e4 (2019).

14. M. L. Truitt, *et al.*, Differential Requirements for eIF4E Dose in Normal Development and Cancer. *Cell* 162, 59 71 (2015).

15. P. Sénéchal, *et al.*, Assessing eukaryotic initiation factor 4F subunit essentiality by CRISPR-induced gene ablation in the mouse. *Cell Mol Life Sci* 78, 6709–6719 (2021).

16. J. R. Graff, *et al.*, Therapeutic suppression of translation initiation factor eIF4E expression reduces tumor growth without toxicity. *J Clin Invest* 117, 2638–2648 (2007).

17. P. Syntichaki, K. Troulinaki, N. Tavernarakis, eIF4E function in somatic cells modulates ageing in Caenorhabditis elegans. *Nature* 445, 922–926 (2007).

18. B.-R. Chen, *et al.*, MNK2-eIF4E axis promotes cardiac repair in the infarcted mouse heart by activating cyclin D1. *J Mol Cell Cardiol* 166, 91–106 (2022).

19. J. Robalino, B. Joshi, S. C. Fahrenkrug, R. Jagus, Two Zebrafish eIF4E Family Members Are Differentially Expressed and Functionally Divergent*. *J Biol Chem* 279, 10532–10541 (2004).

20. N. Minshall, M. H. Reiter, D. Weil, N. Standart, CPEB Interacts with an Ovary-specific eIF4E and 4E-T in Early Xenopus Oocytes*. *J Biol Chem* 282, 37389–37401 (2007).

21. B. Joshi, K. Lee, D. L. Maeder, R. Jagus, Phylogenetic analysis of eIF4E-family members. *Bmc Evol Biol* 5, 48–48 (2005).

22. Y. Zhang, *et al.*, A comparative genomics study of carbohydrate/glucose metabolic genes: from fish to mammals. *Bmc Genomics* 19, 246 (2018).

23. K. Hirose, *et al.*, Evidence for hormonal control of heart regenerative capacity during endothermy acquisition. *Science* 364, 184 188 (2019).

24. W. Wang, *et al.*, Changes in regeneration-responsive enhancers shape regenerative capacities in vertebrates. *Science* 369, eaaz3090 (2020).

25. W. T. Stockdale, *et al.*, Heart Regeneration in the Mexican Cavefish. *Cell Reports* 25, 1997 2007.e7 (2018).

26. S.-L. Lai, *et al.*, Reciprocal analyses in zebrafish and medaka reveal that harnessing the immune response promotes cardiac regeneration. *Elife* 6, 1382 (2017).

27. J. S. Taylor, Y. V. de Peer, I. Braasch, A. Meyer, Comparative genomics provides evidence for an ancient genome duplication event in fish. *Philosophical Transactions Royal Soc Lond Ser B Biological Sci* 356, 1661–1679 (2001).

28. J. Trifinopoulos, L.-T. Nguyen, A. von Haeseler, B. Q. Minh, W-IQ-TREE: a fast online phylogenetic tool for maximum likelihood analysis. *Nucleic Acids Res* 44, W232–W235 (2016).

29. D. Kubacka, *et al.*, Distinct Features of Cap Binding by eIF4E1b Proteins. *J Mol Biol* 427, 387–405 (2015).

30. S. Grüner, *et al.*, The Structures of eIF4E-eIF4G Complexes Reveal an Extended Interface to Regulate Translation Initiation. *Mol Cell* 64, 467–479 (2016).

31. M. Baek, *et al.*, Accurate prediction of protein structures and interactions using a 3-track neural network. *Sci New York N Y* 373, 871–876 (2021).

32. J. Jumper, *et al.*, Highly accurate protein structure prediction with AlphaFold. *Nature* 596, 583–589 (2021).

33. R. J. White, *et al.*, A high-resolution mRNA expression time course of embryonic development in zebrafish. *Elife* 6, e30860 (2017).

34. C. Chapat, *et al.*, Cap-binding protein 4EHP effects translation silencing by microRNAs. *Proc National Acad Sci* 114, 5425–5430 (2017).

35. M. J. Osborne, *et al.*, eIF4E3 acts as a tumor suppressor by utilizing an atypical mode of methyl-7-guanosine cap recognition. *Proc National Acad Sci* 110, 3877–3882 (2013).

36. S. A. Harvey, *et al.*, Identification of the zebrafish maternal and paternal transcriptomes. *Dev Camb Engl* 140, 2703–2710 (2013).

37. M. Altmann, P. P. Müller, J. Pelletier, N. Sonenberg, H. Trachsel, A Mammalian Translation Initiation Factor Can Substitute for Its Yeast Homologue in Vivo. *J Biol Chem* 264, 12145–12147 (1989).

38. B. R. Keegan, J. L. Feldman, G. Begemann, P. W. Ingham, D. Yelon, Retinoic acid signaling restricts the cardiac progenitor pool. *Science* 307, 247 249 (2005).

39. K. Kikuchi, *et al.*, Retinoic acid production by endocardium and epicardium is an injury response essential for zebrafish heart regeneration. *Dev Cell* 20, 397 404 (2011).

40. D. W. Huang, B. T. Sherman, R. A. Lempicki, Systematic and integrative analysis of large gene lists using DAVID bioinformatics resources. *Nat Protoc* 4, 44–57 (2009).

41. B. T. Sherman, *et al.*, DAVID: a web server for functional enrichment analysis and functional annotation of gene lists (2021 update). *Nucleic Acids Res* 50, W216–W221 (2022).

42. L. Sun, *et al.*, EB1 promotes Aurora-B kinase activity through blocking its inactivation by protein phosphatase 2A. *Proc National Acad Sci* 105, 7153–7158 (2008).

43. A. Okuda, G. Kimura, An Amino Acid Change in Novel Protein D123 Is Responsible for Temperature-Sensitive G1-Phase Arrest in a Mutant of Rat Fibroblast Line 3Y1. *Exp Cell Res* 223, 242–249 (1996).

44. A. F. Perzlmaier, F. Richter, W. Seufert, Translation Initiation Requires Cell Division Cycle 123 (Cdc123) to Facilitate Biogenesis of the Eukaryotic Initiation Factor 2 (eIF2). *J Biol Chem* 288, 21537–21546 (2013).

45. J. Lorent, *et al.*, Translational offsetting as a mode of estrogen receptor α-dependent regulation of gene expression. *Embo J* 38, e101323 (2019).

46. E. P. Kusnadi, C. Timpone, I. Topisirovic, O. Larsson, L. Furic, Regulation of gene expression via translational buffering. *Biochimica Et Biophysica Acta Bba - Mol Cell Res* 1869, 119140 (2021).

47. M. Gemberling, R. Karra, A. L. Dickson, K. D. Poss, Nrg1 is an injury-induced cardiomyocyte mitogen for the endogenous heart regeneration program in zebrafish. *Elife* 4 (2015).

48. K. Bersell, S. Arab, B. Haring, B. KUhn, Neuregulin1/ErbB4 signaling induces cardiomyocyte proliferation and repair of heart injury. *Cell* 138, 257 270 (2009).

49. G. D'Uva, *et al.*, ERBB2 triggers mammalian heart regeneration by promoting cardiomyocyte dedifferentiation and proliferation. *Nat Cell Biol* 17, 627 638 (2015).

50. A. Lepilina, *et al.*, A dynamic epicardial injury response supports progenitor cell activity during zebrafish heart regeneration. *Cell* 127, 607 619 (2006).

51. N. Tahara, *et al.*, The FGF-AKT pathway is necessary for cardiomyocyte survival for heart regeneration in zebrafish. *Dev Biol* 472, 30–37 (2021).

52. T. Sakurai, M. Tsuchida, P. D. Lampe, M. Murakami, Cardiomyocyte FGF signaling is required for Cx43 phosphorylation and cardiac gap junction maintenance. *Exp Cell Res* 319, 2152–2165 (2013).

53. R. Fukuda, *et al.*, Stimulation of glycolysis promotes cardiomyocyte proliferation after injury in adult zebrafish. *Embo Rep* 21, e49752 (2020).

54. A. C. Cardoso, *et al.*, Mitochondrial Substrate Utilization Regulates Cardiomyocyte Cell Cycle Progression. *Nat Metabolism* 2, 167–178 (2020).

55. J. W. Miklas, *et al.*, Amino acid primed mTOR activity is essential for heart regeneration. *Iscience* 25, 103574 (2021).

56. K. S. Echtay, *et al.*, Superoxide activates mitochondrial uncoupling proteins. *Nature* 415, 96–99 (2002).

57. A. Bezawork-Geleta, J. Rohlena, L. Dong, K. Pacak, J. Neuzil, Mitochondrial Complex II: At the Crossroads. *Trends Biochem Sci* 42, 312–325 (2017).

58. J.-J. Lin, F.-Y. Wang, W.-H. Li, T.-Y. Wang, The rises and falls of opsin genes in 59 ray-finned fish genomes and their implications for environmental adaptation. *Sci Rep-uk* 7, 15568 (2017).

59. C. Bian, *et al.*, The Asian arowana (Scleropages formosus) genome provides new insights into the evolution of an early lineage of teleosts. *Sci Rep-uk* 6, 24501 (2016).

60. I. Braasch, *et al.*, The spotted gar genome illuminates vertebrate evolution and facilitates human-teleost comparisons. *Nat Genet* 48, 427 437 (2016).

61. X. You, *et al.*, Mudskipper genomes provide insights into the terrestrial adaptation of amphibious fishes. *Nat Commun* 5, 5594 (2014).

62. C. M. Austin, M. H. Tan, L. J. Croft, M. P. Hammer, H. M. Gan, Whole Genome Sequencing of the Asian Arowana (Scleropages formosus) Provides Insights into the Evolution of Ray-Finned Fishes. *Genome Biol Evol* 7, 2885–2895 (2015).

63. B. Q. Minh, *et al.*, IQ-TREE 2: New Models and Efficient Methods for Phylogenetic Inference in the Genomic Era. *Mol Biol Evol* 37, 1530–1534 (2020).

64. T. Gupta, M. C. Mullins, Dissection of Organs from the Adult Zebrafish. *J Vis Exp Jove*, 1717 (2010).

65. Y. Hu, S. Xie, J. Yao, Identification of Novel Reference Genes Suitable for qRT-PCR Normalization with Respect to the Zebrafish Developmental Stage. *Plos One* 11, e0149277 (2016).

66. N. T. Ingolia, G. A. Brar, S. Rouskin, A. M. McGeachy, J. S. Weissman, The ribosome profiling strategy for monitoring translation in vivo by deep sequencing of ribosome-protected mRNA fragments. *Nat Protoc* 7, 1534–1550 (2012).

67. A. Popa, *et al.*, RiboProfiling: a Bioconductor package for standard Ribo-seq pipeline processing. *F1000research* 5, 1309 (2016).

68. M. Lawrence, *et al.*, Software for Computing and Annotating Genomic Ranges. *Plos Comput Biol* 9, e1003118 (2013).

69. M. I. Love, W. Huber, S. Anders, Moderated estimation of fold change and dispersion for RNA-seq data with DESeq2. *Genome Biol* 15, 550 (2014).

70. K. D. Poss, L. G. Wilson, M. T. Keating, Heart regeneration in zebrafish. *Science* 298, 2188 2190 (2002).

71. J. Wang, *et al.*, The regenerative capacity of zebrafish reverses cardiac failure caused by genetic cardiomyocyte depletion. *Development* 138, 3421 3430 (2011).

72. P. A. Peri-Okonny, *et al.*, High-Phosphate Diet Induces Exercise Intolerance and Impairs Fatty Acid Metabolism in Mice. *Circulation* 139, 1422–1434 (2019).

Figure Legends

Fig. 1. Eif4e1c is both unique to and shared by all aquatic vertebrates. Shown is a phylogeny of eIF4E1 orthologues from a sampling of the species considered (see *SI Appendix* Fig. S1 for full analysis). Eif4e1c is ancestral to the canonical eIF4E1A split from its variant, eIF4E1B. Terrestrial species have a canonical and eIF4E1B ortholog (pink and purple). All aquatic species have a canonical variant: 8 species with a duplication (blue and green), 2 species retain only one variant of the duplication, and the *Scyliorhinus canicular* (Small-spotted catshark) canonical clusters with terrestrial eIF4E1A. All 12 aquatic vertebrate retain an Eif4e1c family member. Shown are images of each of the aquatic vertebrate species to highlight the diversity considered. Only 5 of 12 aquatic vertebrate shown here retain an eIF4E1B variant. Estimates are made using maximum likelihood and the IQ-TREE. Nodes with bootstrap support < 0.85 are marked with their respective values, all other nodes had support values of 0.85 or higher.

Fig. 2. Highly conserved Eif4e1c specific amino acids form a novel patch along the surface of the protein. (*A*) ClustalW sequence alignment of human vs fish eif4E orthologs. Highlighted are universally conserved amino acids required for cap binding (green) and eIF4G recruitment (pink). Residues that distinguish EIF4E1A family members (gray) from EIF4E1B family members (black) are also highlighted. The six amino acids most responsible for strong cap binding are marked by red carrots (**^**). The Eif4e1c family conserved residues are highlighted yellow with red letters. The seven residues that are identical in all EIF4E1A and EIF4E1B family orthologs throughout evolution but are uniquely changed in Eif4e1c family members are highlighted in red. Amino acids that diverge between mouse and human are bolded in the human sequence. (*B*) Shown is a PyMol rendition of zebrafish Eif4e1c mapped along the human structure of EIF4E1A bound to a methylated cap (green) and a EIF4G peptide (orange). The tryptophans required for both associations are conserved and highlighted in yellow. All Eif4e1c specific residues are highlighted in red. (*C*) The abundance of each of the transcripts shown in the legend were detected using qPCR on different adult tissues. Expression is determined relative to *mob4* and then normalized to expression levels in the heart. (*D*) Shown is a time course of RNAseq at different developmental stages in embryos. Normalized sequencing reads for the four different EIF4E1 orthologs are shown.

Fig. 3. Δ*eif4e1c* mutants have impaired growth and poor survival. (*A*) Schematic of the CRISPR mediated deletion of *eif4e1c*. Red rectangles represent coding exons, and the white box represents exons with untranslated regions. (*B*) Table showing survival of progeny from crosses of Δeif4e1c heterozygote carriers. Clutches of fish were genotyped at the listed development stage (dpf, wpf and mpf represent days-, weeks- or months-post-fertilization). Significant deviations from Mendelian ratios were calculated using chi^2 and the resulting p-value is shown. (*C*) Fish were grown together, genotyped at the listed stage (top label) and immediately measured from jaw to the caudal fin bifurcation (3-month average = 1.82 and 1.62; Welch's t-test, p-value = 0.0156, n=24 vs 23; 6-month average = 2.48 and 2.37; Welch's t-test, p-value = ns, n=20 vs 20). (*D*) After measuring length, fish were dried off as much as possible and weighed (3-month average = 146.5mg and 103.1mg; Welch's t-test, p-value = 0.0014, n=24 vs 23; 6-month average = 344.6 and 261.7; Welch's t-test, p-value = 0.0002, n=20 vs 20). (*E*) Uninjured heart ventricles from wildtype and mutant fish were sectioned and stained for muscle using antibodies toward the Myosin heavy chain (MHC) and the cardiac transcription factor Mef2c to identify CM nuclei. The numbers of Mef2c positive cells were counted with MIPAR (average = 3070 and 2432; Welch's t-test, p-value = 0.0054, n=10 vs 8).

Fig. 4. Ribosome profiling indicates translational changes in *eif4e1c* mutant hearts. (*A*) Shown is a cartoon of ribosome profiling. Ribosome bound mRNA is purified from wildtype and mutant hearts and then subjected to micrococcal nuclease (Mnase) digestion. Fragments of mRNA protected by being bound by ribosomes are then purified and subjected to high-throughput sequencing. (*B*) Differences in mRNA abundance (log_2) are plotted versus changes in the abundance of ribosome protected fragments (RPF). Genes whose translation does not change significantly are plotted in gray, genes where translation is decreasing in the mutant are plotted in red and those genes where translation is increasing in the mutant are plotted in blue. Decreasing genes mentioned in the text are colored gold and increasing genes mentioned in the text are colored green. (*C*) Shown are high-throughput sequencing browser tracks for four genes (blue arrows) that are important for CM proliferation (*stat3*) or progression of the cell-cycle (*plk3*, *cdc123*, and *mapre1a*). Wildtype (WT) data is shown in blue, and mutant (MUT) data is shown in green. The top two tracks (mRNA) represent abundance of transcript measured from RNAseq of the input material and the bottom two tracks are the abundance of ribosome protected fragments (RPF). (*D*) Shown is a time-course of oxygen consumption rates (OCR) from mitochondria measured by the Seahorse analyzer. Hashed lines indicate time points of drug injection. Readings were normalized to the number of mitochondria using qPCR. The first injection (I1) is of ADP to stimulate respiration, the second injection (I2) is of oligomycin to inhibit ATP synthase (complex V) decreasing electron flow through transport chain, the third injection (I3) is of FCCP to uncouple the proton gradient, and the fourth injection (I4) is of antimycin A to inhibit complex III to shut down mitochondrial respiration. (*E*) Basal respiration is calculated as the OCR average after addition of ATP (I1 to I2) subtracting the non-mitochondrial respiration after injection of antimycin A (after I4) (mean = 60.01 and 42.25; Welch's t-test, p value < 0.0001; N= 15,15). Maximal respiration is calculated as the OCR average after FCCP addition (I3 to I4) subtracting the non-mitochondrial respiration after injection of antimycin A (after I4) (mean = 68.73 and 52.19; Welch's t-test, p value < 0.0001; N= 15,15).

Fig. 5. Deletion of *eif4e1c* impairs CM proliferation in regenerating hearts. (*A*) Images of sectioned amputated ventricles (7dpa) from wildtype and Δ*eif4e1c* mutant fish. Sections are stained for Mef2c (green) and EdU (red). Below – double positive cells are highlighted in black using a MIPAR software rendition. On the right is a graph of quantification of CM proliferation indices (Mef2/EdU double positive over total Mef2 positive) in 7dpa ventricles (average = 10.68 and 6.02; Welch's t-test, **p-value = .0054, n= 11 vs 13). (*B*) Cryosections of fresh mutant and wildtype hearts were stained for Succinate dehydrogenase activity. Shown are uninjured hearts (top row) and hearts that were ablated genetically using ZCAT (7 days-post-incubation). (*C*) The mean signal intensity was calculated per given area for Sdh stained hearts (Uninjured average = 7.47 and 7.57 with N = 6 vs 8; Regeneration average = 4.59 and 5.06 with N = 4 vs 4). The Welch's t-test was used to calculate significance (wildtype vs mutant uninjured = .781, wildtype uninjured vs wildtype regeneration **** < 0.0001, mutant uninjured vs mutant regeneration **** < 0.0001, wildtype vs mutant during regeneration * = .0416). (*D*) Cartoon of caudal fin regeneration experiments. The blastema is the highly proliferative zone of growth that forms the new fin. (*E*) Caudal fins were amputated ~50% in Δ*eif4e1c* mutants and their wildtype siblings and fin ray regrowth was determined 4 days later. There was no significant difference between the groups (average = 849.6μm and 857.2μm; Welch's t-test, p-value =0.8605, N = 30 vs 25).

Supplemental Figures

Figure S1 Phylogeny and conservation of eif4E orthologs.
(*A*) Shown is the phylogeny of Eif4e1c orthologues (all 53 species with 142 homologs) estimated using maximum likelihood using IQ-TREE. Nodes with bootstrap support < 0.85 are marked with their respective values, all other nodes had support values of 0.85 or higher. (*B*) ClustalW sequence alignment of Eif4e1c from aquatic vertebrate. Species names are color-coded by type with the legend on the bottom. Conserved Eif4e1c specific residues are highlighted in red bold with similar residues highlighted in pink.

Figure S2
Heterozygotes for Δ*eif4e1c* were compared for length and weight with their wildtype siblings. (*A*) Fish were grown together, genotyped at the listed stage (top label) and immediately measured from jaw to the caudal fin bifurcation (Average length = 2.15 and 2.15 with N=31 vs 37; Welch's t-test, p-value =.963,). After measuring length, fish were dried off as much as possible and weighed (Average weight = 181.0 and 180.7 with N=31 vs 37; Welch's t-test, p-value = .978,). (*B*) CM numbers for wildtype and Δ*eif4e1c* mutants were counted at 6mpf from cryosections stained with an antibody for Mef2c. The numbers of Mef2c positive cells were counted with MIPAR (average = 6061 and 4557 with N = 7 vs 7; Welch's t-test, p-value = 0.0055).

Figure S3
(*A*) Gene ontology categories were discovered using the DAVID on-line platform. Each category is listed on the left with the identifier in parentheses. Shown are GO categories with p-value < .05 (indicated by dotted line). X-axis is $-\log_{10}$(p-value). Parentheses to the right of the bar indicate numbers of genes identified in each group. (*B*) Cartoon depicting experimental set-up for Seahorse analysis. Mitochondria were isolated from hearts dissected from wildtype and mutant fish and then processed on the Seahorse analyzer from Agilent. (*C*) Shown is a time-course of oxygen consumption rates (OCR) from mitochondria measured by the Seahorse analyzer. Hashed lines indicate time points of drug injection. The first injection (I1) is of ADP to stimulate respiration, the second injection (I2) is of oligomycin to inhibit ATP synthase (complex V) decreasing electron flow through transport chain, the third injection (I3) is of FCCP to uncouple the proton gradient, and the fourth injection (I4) is of antimycin A to inhibit complex III to shut down mitochondrial respiration. (*D*) Basal respiration is calculated as the OCR average after addition of ATP (I1 to I2) subtracting the non-mitochondrial respiration after injection of antimycin A (after I4) (mean = 85.30 and 20.90; Welsh's t-test p value < 0.0001; N= 15,18). (*E*) Maximal respiration is calculated as the OCR average after FCCP addition (I3 to I4) subtracting the non-mitochondrial respiration after injection of antimycin A (after I4) (mean = 74.64 and 28.34; Welsh's t-test p value < 0.0001; N= 15,18).

Figure S4
(*A*) Images of sectioned ventricles at 28dpa are stained for Myosin heavy chain (MHC) to indicate cardiac muscle. Shown below are the same sections stained with AFOG which shows muscle (orange), Fibrin (red) and Collagen (blue). Hearts from 5 wildtype and 5 Δ*eif4e1c* mutants were ranked by injury size. Shown are representative hearts that were in the middle of the groups. (*B*) Caudal fins were amputated ~50% and the blastema were imaged 48 hours later for Δ*eif4e1c* mutants and their wildtype siblings. The length of the blastema was measured from the tip of the 3rd ray using the Zeiss microscope software. There was no significant difference between the groups (2dpa average = 0.0151mm and 0.0146mm; Welsh's t-test, p-

value = 0.656, N = 18 vs 22; 4dpa average = 0.0539 and 0.0545; Welsh's t-test, p-value = 0.890, N = 12 vs 16). (*C*) qPCR was performed for *eif4e1aa* (pink), *eif4e1ab* (blue), *eif4e1c* (black) on fins during regeneration. Ct values were normalized to *mob4*, a gene does not change levels between cell types or conditions. Relative expression changes during regeneration (Regen Induced) are shown for wildtype (WT) and mutant (MUT) fins as the normalized Ct during regeneration over normalized Ct from uninjured fins (two groups on the left). The same data is represented a second way on the right as relative expression differences between mutants and wildtype siblings (Mut vs WT) during regeneration (Regen) and in the uninjured (Uninj). (*D*) same experimental set-up as in (*C*) but performed on adult hearts.

Figure S5

(*A*) Shown are the correlations between replicates for ribosome profiling (top) and RNAseq of the inputs (bottom) for both wildtype (left) and Δ*eif4e1c* mutant (right) samples.

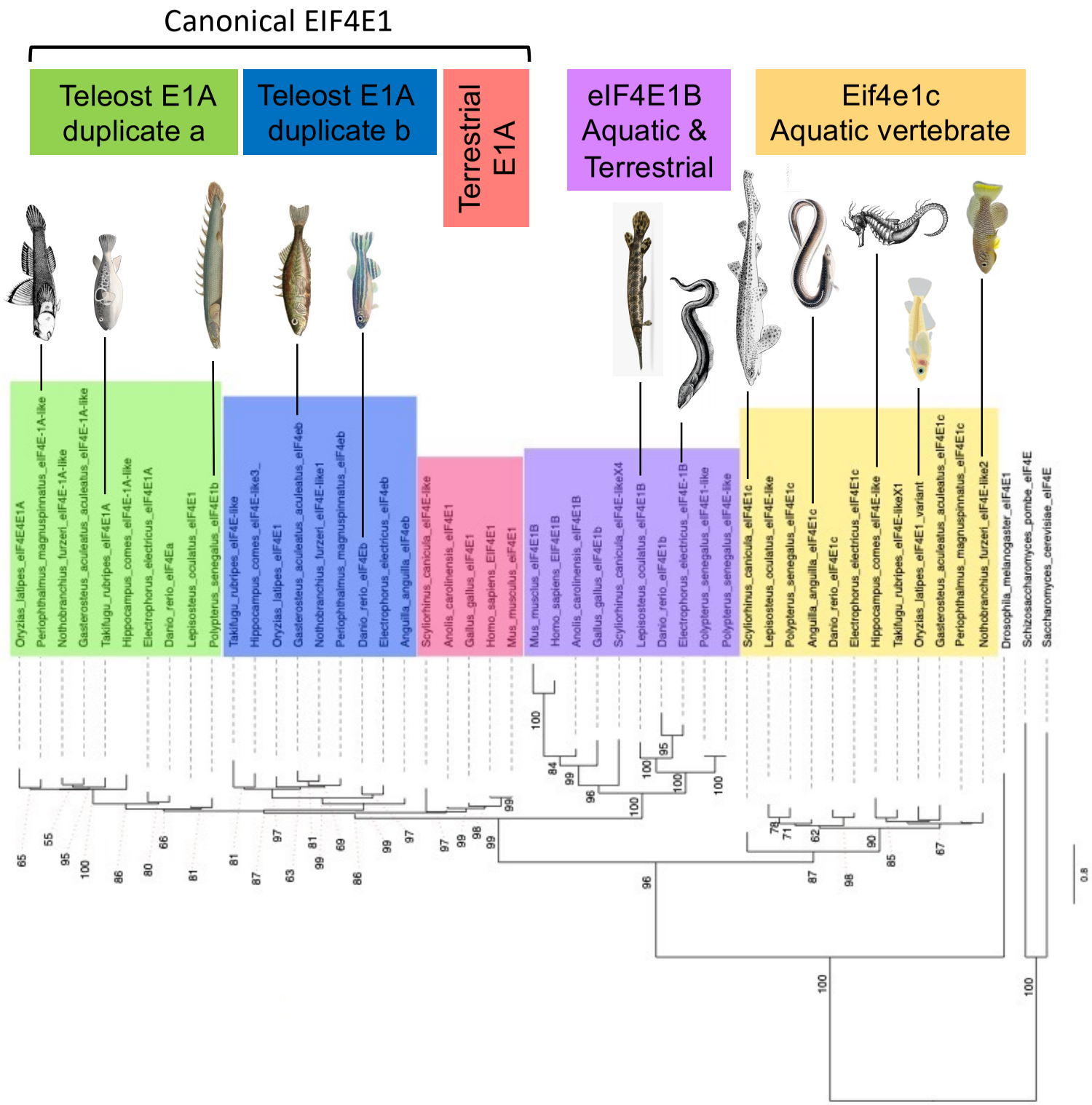
Canonical EIF4E1
Teleost E1A duplicate a
Teleost E1A duplicate b
Terrestrial E1A
eIF4E1B Aquatic & Terrestrial
Eif4e1c Aquatic vertebrate
Oryzias_latipes_eIF4E4E1A
Periophthalmus_magnuspinnatus_eIF4E-1A-like
Nothobranchius_furzeri_eIF4E-1A-like
Gasterosteus_aculeatus_aculeatus_eIF4E-1A-like
Takifugu_rubripes_eIF4E1A
Hippocampus_comes_eIF4E-1A-like
Electrophorus_electricus_eIF4E1A
Danio_rerio_eIF4Ea
Lepisosteus_oculatus_eIF4E1
Polypterus_senegalus_eIF4E1b
Takifugu_rubripes_eIF4E-like
Hippocampus_comes_eIF4E-like3_
Oryzias_latipes_eIF4E1
Gasterosteus_aculeatus_aculeatus_eIF4eb
Nothobranchius_furzeri_eIF4E-like1
Periophthalmus_magnuspinnatus_eIF4eb
Danio_rerio_eIF4Eb
Electrophorus_electricus_eIF4eb
Anguilla_anguilla_eIF4eb
Scyliorhinus_canicula_eIF4E-like
Anolis_carolinensis_eIF4E1
Gallus_gallus_eIF4E1
Homo_sapiens_EIF4E1
Mus_musculus_eIF4E1
Mus_musclus_eIF4E1B
Homo_sapiens_EIF4E1B
Anolis_carolinensis_eIF4E1B
Gallus_gallus_eIF4E1b
Scyliorhinus_canicula_eIF4E-likeX4
Lepisosteus_oculatus_eIF4E1B
Danio_rerio_eIF4E1b
Electrophorus_electricus_eIF4E-1B
Polypterus_senegalus_eIF4E1-like
Polypterus_senegalus_eIF4E-like
Scyliorhinus_canicula_eIF4E1c
Lepisosteus_oculatus_eIF4E-like
Polypterus_senegalus_eIF4E1c
Anguilla_anguilla_eIF4E1c
Danio_rerio_eIF4E1c
Electrophorus_electricus_eIF4E1c
Hippocampus_comes_eIF4E-like
Takifugu_rubripes_eIF4E-likeX1
Oryzias_latipes_eIF4E1_variant
Gasterosteus_aculeatus_aculeatus_eIF4E1c
Periophthalmus_magnuspinnatus_eIF4E1c
Nothobranchius_furzeri_eIF4E-like2
Drosophila_melanogaster_eIF4E1
Schizosaccharomyces_pombe_eIF4E
Saccharomyces_cerevisiae_eIF4E
0.8

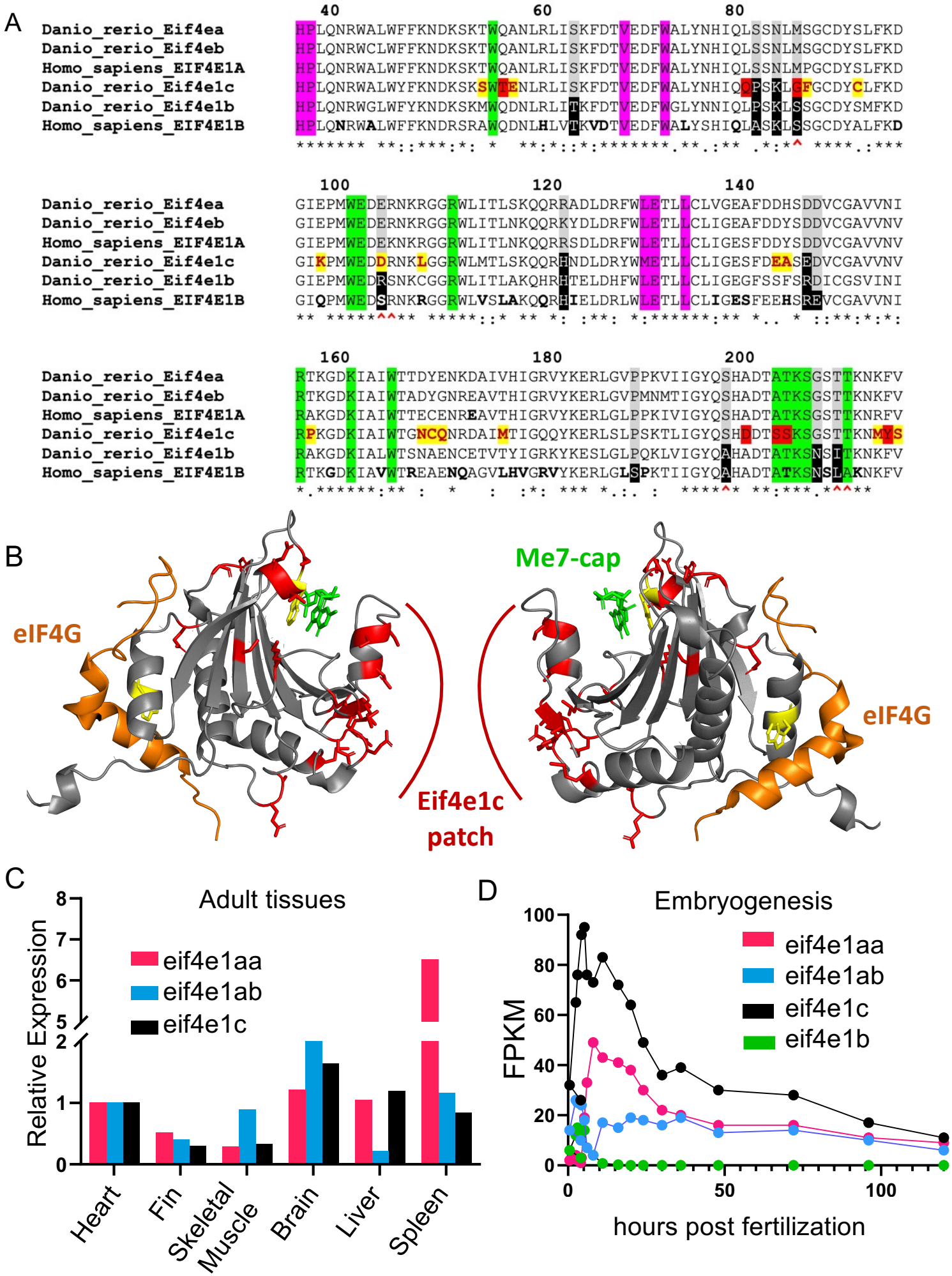
A
40
60
80
Danio_rerio_Eif4ea
Danio_rerio_Eif4eb
Homo_sapiens_EIF4E1A
Danio_rerio_Eif4e1c
Danio_rerio_Eif4e1b
Homo_sapiens_EIF4E1B
100
120
140
160
180
200
B
eIF4G
Me7-cap
eIF4G
Eif4e1c
patch
C
Adult tissues
Relative Expression
eif4e1aa
eif4e1ab
eif4e1c
Heart
Fin
Skeletal
Muscle
Brain
Liver
Spleen
D
Embryogenesis
FPKM
eif4e1aa
eif4e1ab
eif4e1c
eif4e1b
hours post fertilization

A

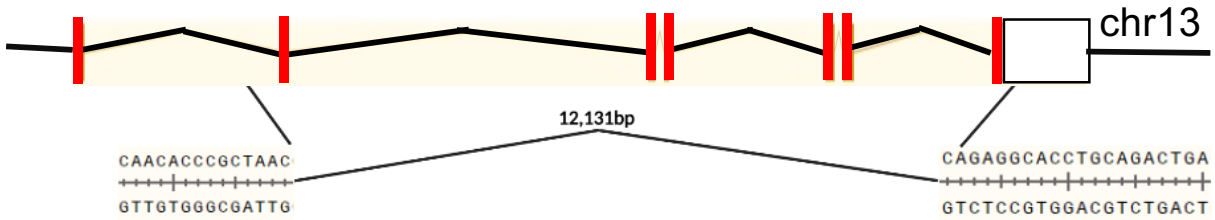

B

Cross	Stage	N	WT	HETS	HOMS	chi²	p value	Significant?
Δeif4e1c HETS X HETS	3dpf	190	51	85	54	1.94	0.33	no
	4wpf	410	109	203	98	0.629	0.73	no
	8wpf	630	207	312	111	29.3	4.31E-07	yes
	>3mpf	1868	599	951	318	84.9	3.22E-19	yes
Δeif4e1c HOMS ♀ X HETS ♂	3dpf	107	N/A	58	49	0.757	0.384	no

C

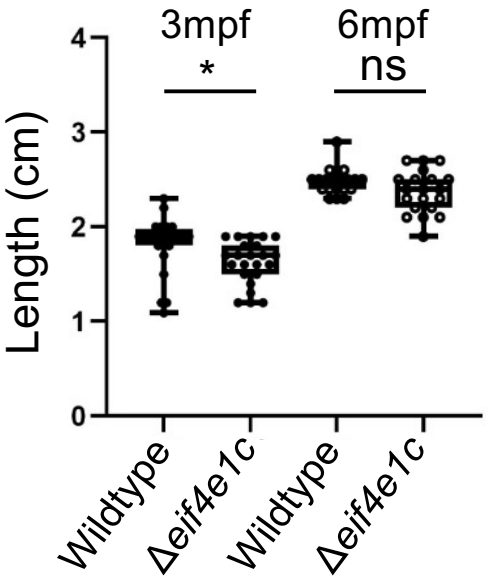

D

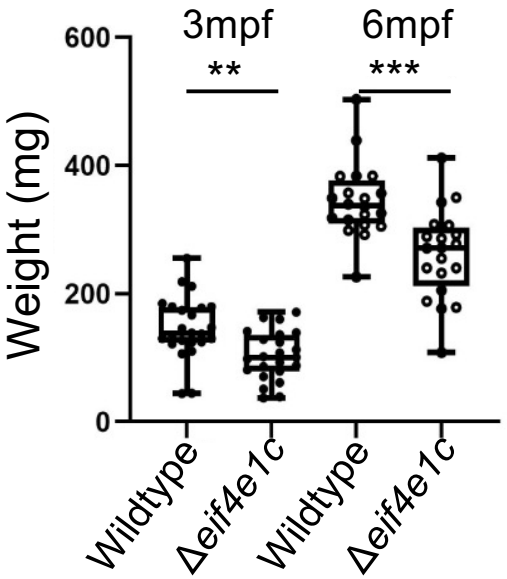

E

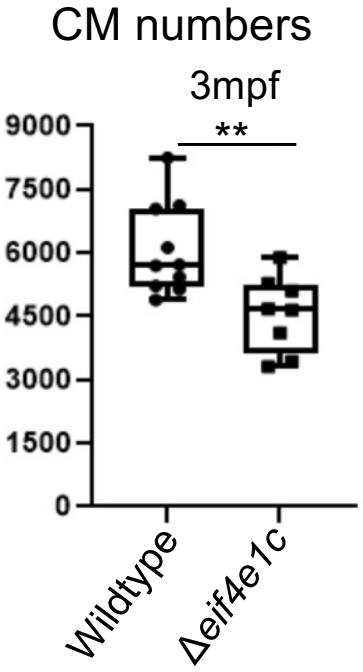

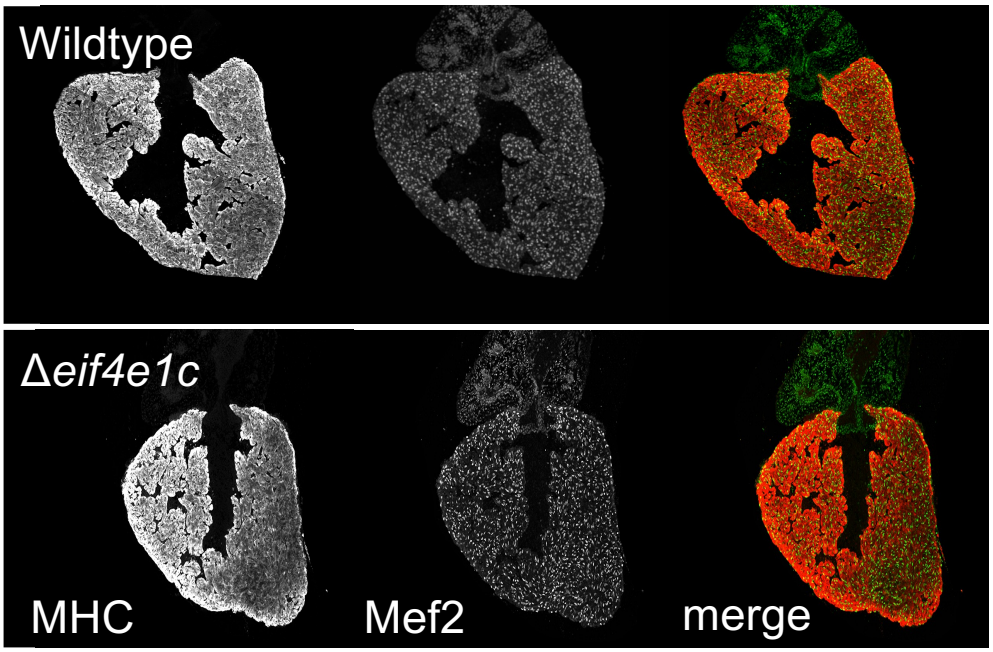

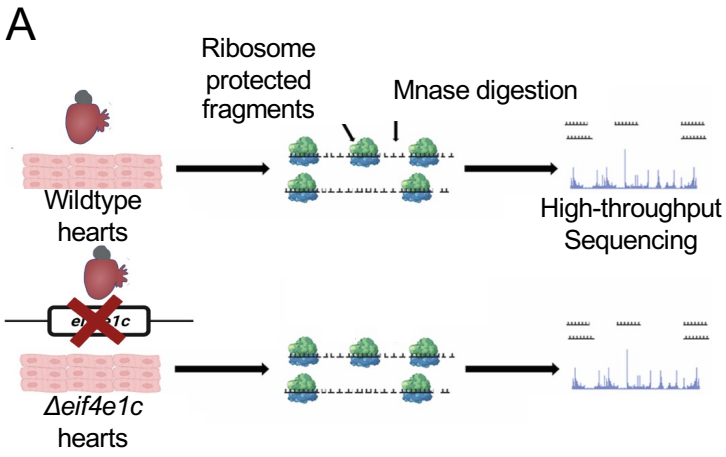
A
Ribosome protected fragments
Mnase digestion
Wildtype hearts
High-throughput Sequencing
Δeif4e1c hearts

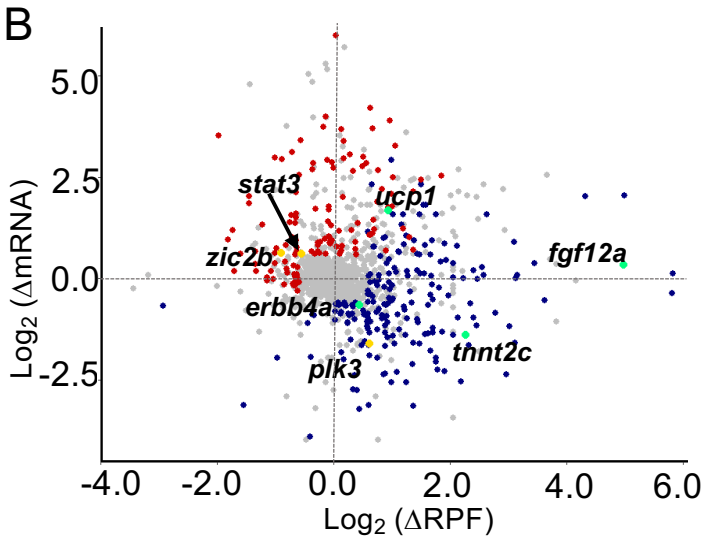
B
5.0
2.5
0.0
-2.5
-4.0
-2.0
0.0
2.0
4.0
6.0
Log2 (ΔmRNA)
Log2 (ΔRPF)
stat3
ucp1
zic2b
fgf12a
erbb4a
plk3
tnnt2c

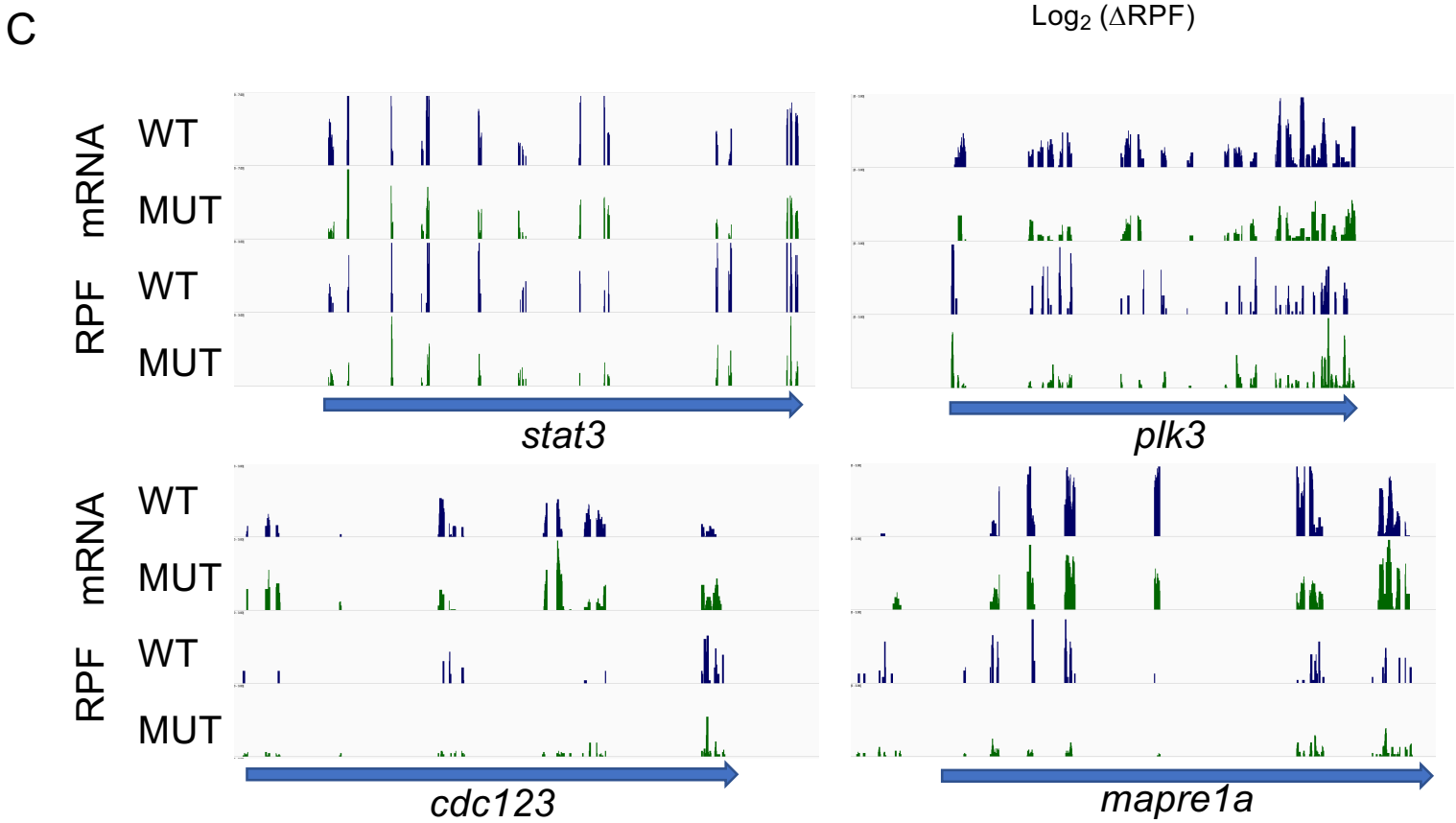
C
mRNA
RPF
WT
MUT
WT
MUT
stat3
plk3
mRNA
RPF
WT
MUT
WT
MUT
cdc123
mapre1a

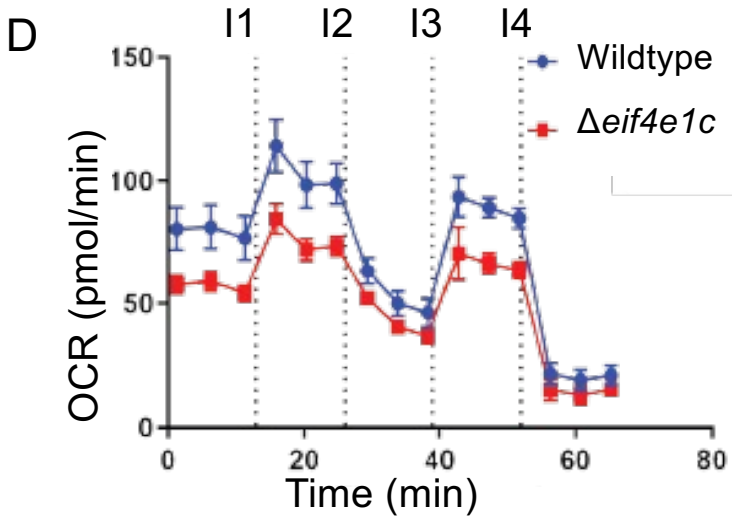
D
I1
I2
I3
I4
Wildtype
Δeif4e1c
150
100
50
0
OCR (pmol/min)
0
20
40
60
80
Time (min)

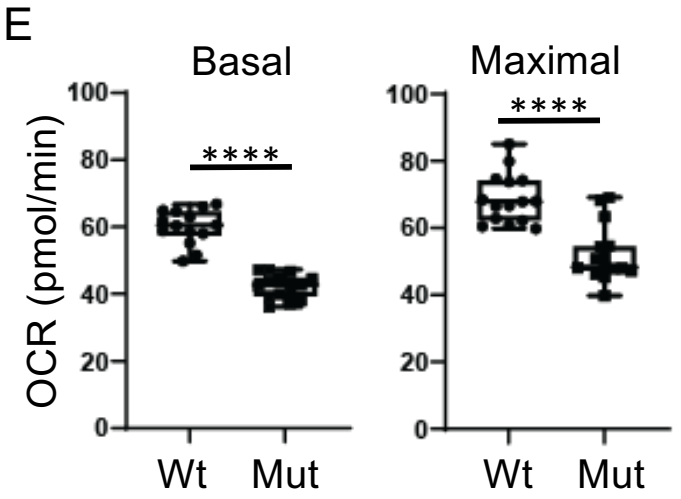
E
Basal
Maximal
****
****
100
80
60
40
20
0
OCR (pmol/min)
Wt
Mut
Wt
Mut

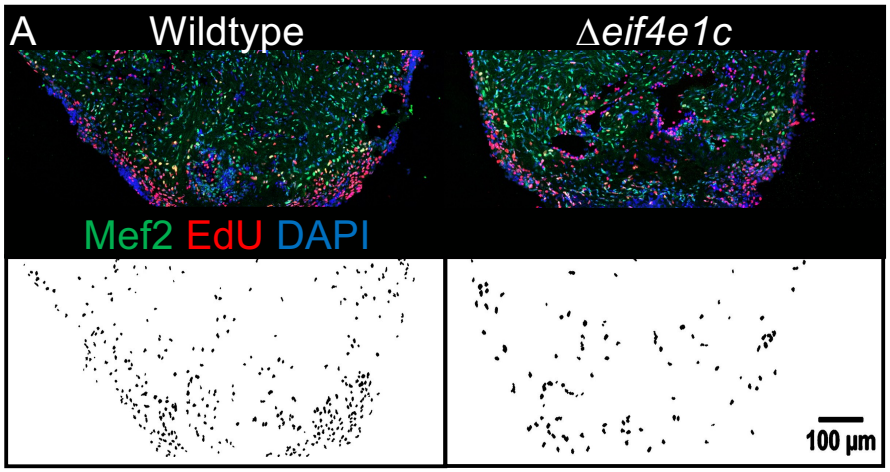
A
Wildtype
Δeif4e1c
Mef2 EdU DAPI
100 µm

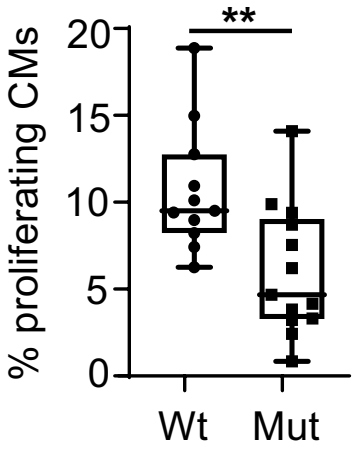
% proliferating CMs
20
15
10
5
0
**
Wt
Mut

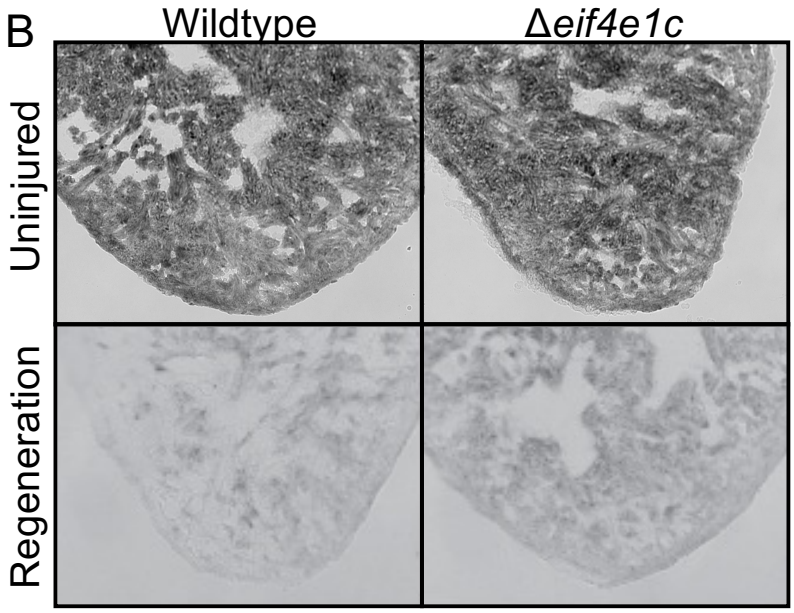
B
Wildtype
Δeif4e1c
Uninjured
Regeneration

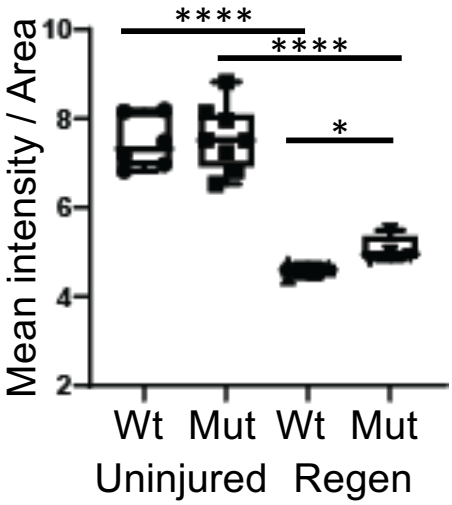
C
Mean intensity / Area
10
8
6
4
2
****
****
*
Wt
Mut
Wt
Mut
Uninjured
Regen

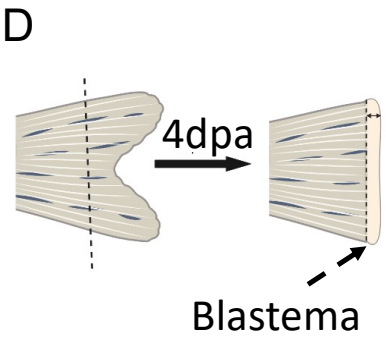
D
4dpa
Blastema

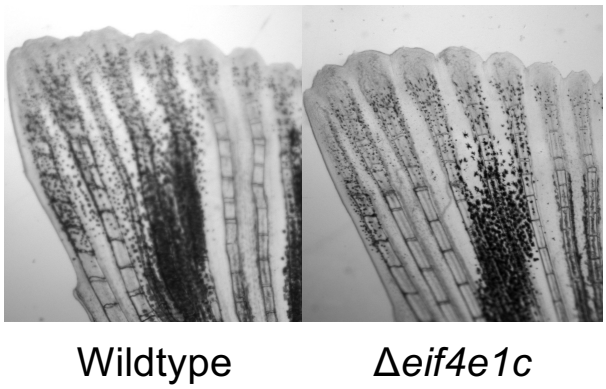
E
Wildtype
Δeif4e1c

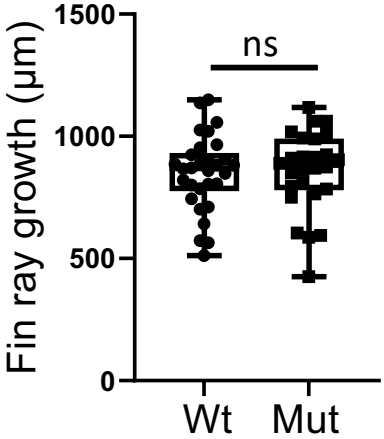
Fin ray growth (µm)
1500
1000
500
0
ns
Wt
Mut